Supplemental Materials:
Sex differences in human adipose tissue gene expression and genetic regulation involve adipogenesis

Warren D. Anderson [1], Joon Yuhl Soh [1], Sarah E. Innis [2], Alexis Dimanche [3], Lijiang Ma [4], Carl D. Langefeld [5], Mary E. Comeau [5], Swapan K. Das [6], Eric E. Schadt [4], Johan L.M. Björkegren [4], and Mete Civelek [1,2]

1: Center for Public Health Genomics, University of Virginia, Charlottesville, VA, USA
2: Department of Biomedical Engineering, University of Virginia, Charlottesville, VA, USA
3: Physics Department, Southwestern University, Georgetown, TX, USA
4: Genetics and Genomic Sciences, Icahn School of Medicine at Mount Sinai, New York, NY, USA
5: Department of Biostatistics and Data Science, Division of Public Health Sciences, Wake Forest University School of Medicine, Winston-Salem, NC, USA
6: Department of Internal Medicine, Section of Endocrinology and Metabolism, Wake Forest University School of Medicine, Winston-Salem, NC, USA
*contact: warrena@virginia.edu and mete@virginia.edu

Outline

Supplemental Methods

Our analyses were predominantly completed using R (R Core Team, 2018) and the Unix command line. Further analysis details can be obtained through a publicly available repository of vignettes and associated scripts (`https://github.com/WarrenDavidAnderson/manuscriptCode/tree/master/sexDifferencesAdipose_code`, see also Supplemental Code).

Analyses of sex differences in gene expression

Evaluation of differential gene expression in human subcutaneous adipose tissue: We downloaded the deCODE and AAGMEx data from `GEO` using R. The deCODE data were approximately normally distributed for a given gene. Sex annotation was not available for deCODE, so we defined sex based on an assessment of the bimodal distribution of *XIST* expression values (Supplemental Fig S1A). *XIST* is a non-coding transcript from the X chromosome, implicated in X-inactivation, and is exclusively expressed in females. Therefore, it is common to assess *XIST* expression to operationally define sample sex or rule out sample annotation errors (Toker et al., 2016; Broman et al., 2015; 't Hoen et al., 2013). The AAGMEx data were accompanied by sex annotation, however, the gene expression distributions were not approximately normal. The general absence of normality was determined by an assessment of the expression quantiles (`https://www.ncbi.nlm.nih.gov/geo/geo2r/`). Hence, we log2 transformed the AAGMEx data. In general, for all of our analyses, we routinely inspected sample-to-sample correlations and removed individual samples from pairs with aberrantly high correlations. We verified all sex annotations by examining *XIST* expression and we removed samples with questionable *XIST* levels (Supplemental Fig S1B,C).

We processed the v8 GTEx gene expression data following the publicly available analysis pipeline from the GTEx Consortium (`https://github.com/broadinstitute/gtex-pipeline`) (GTEx Consortium et al., 2017) and our previous work (Civelek et al., 2017). The data were downloaded in the transcripts per million (TPM) format. We verified the reported sex annotations by analyzing *XIST* expression, as described above. We verified that quantile normalization exerted minimal effects on the TPM data and we omitted sample-based normalization. We inverse-normal transformed the data by mapping the expression ranks of each gene onto a standard normal cdf and applied the inverse transformation, thereby generating a normal distribution of expression levels for each gene. Note that data normalization approaches such as the inverse-normal transform can impose constraints on the observed fold changes for comparisons between two groups. Below we describe an analysis of the inverse-normal transformation, in the context of identifying differential expression fold changes, to illustrate the impact of normalization on the interpretation of differential expression effect magnitudes (Supplemental Fig S2).

To correct for both known and unknown covariates, we utilized surrogate variable analysis (SVA) (Leek and Storey, 2007). We estimated surrogate variables that were distinct from sex, age, RNA integrity number (RIN), and platform. That is, we identified SVs from the residuals obtained by linearly regressing the gene expression levels against sex, age, RIN, and platform, where sex and platform were coded as dummy variables or factors. This analysis identified 36 latent factors (i.e., the SVs). To adjust the data, we implemented multivariate linear regression of the inverse transform normalized gene expression levels with respect to age, RIN, platform, and the 36 latent factors. We retained the residuals for downstream gene expression analysis. We applied principal components analysis (PCA) to verify that this approach effectively corrected the data for both explicitly modeled and un-modeled covariates, while accentuating sex differences in gene expression (Supplemental Fig S3).

We applied the Linear Models for Microarray Data (`Limma`) analysis to evaluate differential gene expression between males and females (Ritchie et al., 2015). According to this method, the standard t-test was applied for each gene. Then the function eBayes() was used to adjust the t-statistics for gene to gene variance fluctuations. The p-values corresponding to the moderated t-statistics were then subjected

to correction for multiple testing using the Benjamini-Hochberg method for determining false discovery rates (FDRs) (Ritchie et al., 2015; Benjamini and Hochberg, 1995).

We evaluated tissue specificity by performing sex-based differential gene expression analysis to GTEx samples from the following tissues: visceral adipose tissue (320 males, 149 females), liver (146 males, 62 females), skeletal muscle (469 males, 237 females), cardiac atrial appendage (253 males, 119 females), cardiac left ventricle (264 males, 122 females), whole blood (441 males, 229 females), and 13 brain regions (78-151 males, 33-64 females). We completed all analyses as described above for the subcutaneous adipose tissue GTEx samples.

We evaluated the obesity-specificity of gene expression sex differences by performing sex-based differential gene expression analysis of samples from subcutaneous adipose tissues of obese gastric bypass patients (Mass General Hospital, MGH, main text Table 1) (Greenawalt et al., 2011). The microarray gene expression data were processed and normalized as described previously (Greenawalt et al., 2011). Annotation for subject sex was not publicly available, so we operationally defined sex based on *XIST* expression. We completed the differential expression analysis using `Limma` (Ritchie et al., 2015), as described above.

Gene set enrichment analysis (`GSEA`): The `GSEA` method evaluates enrichments for gene set annotations (e.g., signaling pathways) in genes that tend to be differentially expressed, without applying a statistical constraint on the degree of differential expression. Rather, `GSEA` determines permutation-based FDRs related to the degree of overlap for the annotations and the most highly differentially expressed genes (Subramanian et al., 2005; Mootha et al., 2003). We implemented `GSEA` using a modified version of publicly available R code (`https://www.gsea-msigdb.org/gsea`). We evaluated functional enrichment in genes with elevated expression in females relative to males using the signal to noise ratio, $(\mu_F - \mu_M)/(\sigma_F + \sigma_M)$ (μ = mean, σ = standard deviation, M = male, F = female). According to this formulation, positive enrichment scores are indicative of functional enrichments for genes elevated in females, whereas negative enrichment scores are indicative of functional enrichments for genes elevated in males. We evaluated enrichments for annotations from the hallmark gene set collection (Liberzon et al., 2015), as well as additional gene sets. The additional gene sets included transcription factor binding targets (ENCODE Project Consortium, 2012), receptors along with associated ligands (Kadoki et al., 2017), and trans-eQTL genes associated with *KLF14* (Small et al., 2018; Civelek et al., 2017).

Functional enrichment analysis with Fisher's Exact Test (FET): The FET facilitates the calculation of an exact p-value corresponding to the significance of deviations from random expectation in a contingency table (Fisher, 1922). This test is used to determine whether particular input gene sets (e.g., differentially expressed genes that satisfy specific statistical criteria) are enriched for specific functional annotations (e.g., cellular components or cell signaling pathways). The `Enrichr` tool was developed to integrate an expansive repertoire of functional annotations with an automated calculation of the corresponding FET p-values and associated FDRs for a given input gene set, with a background consisting of all human genes (Kuleshov et al., 2016; Chen et al., 2013). We completed our FET analyses using the `enrichR` library for R (`https://cran.r-project.org/web/packages/enrichR`). In general, the FET provides an independent alternative to GSEA for evaluating gene set enrichments. In particular, the FET analysis is constrained to specific input gene sets, whereas `GSEA` takes all genes into account, based on their respective degrees of differential expression.

Binding Analysis for Regulation of Transcription (`BART`): `BART` refers to a data-driven method for inferring transcription factors with predicted regulatory influences on gene sets of interest. First, this approach entails identifying putative regulatory regions of DNA associated with a gene list, and estimating the corresponding degrees of regulatory influences, using histone-3 lysine-27 acetylation (H3K27ac) chromatin immunoprecipitation sequencing (ChIP-seq) data (Wang et al., 2016). This approach generates

a cis regulatory profile for each gene. Second, the cis regulatory profiles of gene-proximal regions are integrated with transcription factor ChIP-seq data. The overlaps between cis regulatory regions and factor binding regions are taken as 'true positives' for predictions of binding based on regulation. The area under the receiver operating characteristic curve, or the AUC for the ROC curve, is the dependent measure for a factor's regulatory influence on a given gene. Statistical analyses yield Wilcoxon rank-sum test statistics and associated p-values for comparisons between AUCs for individual factors with AUCs from a null data set (Wang et al., 2018). We computed FDRs from these p-values (Benjamini and Hochberg, 1995). A novel attribute of this approach is the utilization of active enhancer mark H3K27ac genomic distribution data to identify and quantify regulatory regions in a data-driven manner, in tandem with veritable transcription factor binding data from ChIP experiments. In contrast, previous approaches to identify putative regulatory transcription factors were exclusively based on either consensus motifs or ChIP data (Lachmann et al., 2010; Vadigepalli et al., 2003).

STARNET gene expression analysis: We evaluated gene expression measurements from the Stockholm-Tartu Atherosclerosis Reverse Network Engineering Task (STARNET) cohort of healthy individuals from Estonia (main text Table 1). For this cohort, subcutaneous adipose tissue biopsies were obtained from subjects that underwent extensive clinical phenotyping (Franzén et al., 2016). Details regarding sample acquisition and RNA sequencing have been published (Franzén et al., 2016). For our analyses, we focused on the 162 genes identified from our differential expression analyses of the AAGMEx, deCODE, and GTEx cohorts (see main text Fig 1). We log2 transformed the expression data and adjusted the expression for body mass index using linear regression. We performed differential gene expression analysis using `Limma`.

Evaluation of differential gene expression in murine adipose tissue: We evaluated sex-based differential gene expression in the Hybrid Mouse Diversity Panel (HMDP) of inbred mouse strains (GEO accession: GSE64769) (Lusis et al., 2016; Civelek et al., 2017). We considered 98 strains for which there were both female and male epididymal adipose tissue gene expression data. Microarray analysis and normalization has been described previously (Civelek et al., 2017). We completed the differential expression analysis using `Limma` (Ritchie et al., 2015).

Analysis of sex-by-genotype interactions in human

Cis eQTL analysis for sex-by-SNP interactions: We obtained genotype data for the multi-ethnic GTEx cohort from dbGAP (`https://www.ncbi.nlm.nih.gov/projects/gap/cgi-bin/study.cgi?study_id=phs000424.v8.p2`). We filtered the whole genome sequencing genotype data based on minor allele frequency (MAF; excluding SNPs with MAF < 0.05), Hardy-Weinberg equilibrium (HWE, excluding SNPs with HWE exact test p-value $< 1 \times 10^{-6}$), and the proportion of missing data (maximum missing samples = 2%) using `VCFtools` (Danecek et al., 2011). We excluded any sites that did not pass the filters implemented in the original GTEx analysis.

Similar to our expression data processing methods for differential gene expression analysis (Fig S3), we identified covariates that could be used for adjusting the data to augment the sensitivity for detecting eQTLs. We considered three genotype principal components (PCs) to account for the effects of population structure in our eQTL analyses (Price et al., 2006; Patterson et al., 2006). We identified residuals for a linear model of gene expression as a function of three genotype PC score vectors, platform (factor), RIN, age, and sex (factor). Hence, these residuals contained minimal influences of sex. Given these residuals, we applied the probabilistic estimation of expression residuals (`PEER`) analysis to identify latent factors (i.e., PEER factors) independent of the elements in the aforementioned regression model from which we obtained the residuals (Stegle et al., 2012). Following previous approaches (Civelek et al., 2017), we empirically determined that interaction eQTL detection sensitivity was optimized for an analysis using 32

PEER factors as covariates. We verified that the PEER factors were not correlated with either RIN or age, as these variables were 'regressed out' before identifying PEER factors from the residuals.

To determine whether adjusting for PEER factors could facilitate the identification of sex differences in genetic associations with gene expression, we obtained residuals from a linear model with gene expression as a function of three genotype PCs, platform, RIN, age, and 32 PEER factors. We subjected the residuals to PCA and visualized the PC scores in the first two dimensions. The first two PCs captured little variability (1-3%. Supplemental Fig S4), indicating that the PEER correction abrogated much of the existing structure in the data, as was the case for surrogate variable-based correction (Supplemental Fig S3). We annotated the data for covariates that were explicitly modeled, as well as those that were not. The explicit adjustment for age and RIN apparently nullified the influences of these covariates on the first PC. The effects of death circumstance (Hardy scale metric) were also removed, thereby suggesting that PEER effectively corrected for such consistent influences on the data structure by identifying latent factors. However, as the data were corrected for the categorical sex variable before implementing PEER, correcting for the PEER factors left the influence of sex both intact and poignant. Sex could account for the prominent separation of two data clouds along the first PC, indicating that sex was a key variable contributing to the systematic variation in the adjusted data (Supplemental Fig S4). This analysis revealed that adjusting the expression data for set of covariates and PEER factors removed confounding sources of variation while accentuating sex differences (Supplemental Fig S4).

We evaluated sex-by-genotype interactions underlying subcutaneous adipose tissue gene expression, using the GTEx expression data, by associating genotypes at specific SNPs with the expression of genes within 1Mb of the transcription start sites. We used linear models with sex-by-SNP interactions (Gilks et al., 2014; Yao et al., 2014). We performed the expression quantitative trait locus (eQTL) analysis using `Matrix eQTL` (Shabalin, 2012). We implemented this interaction eQTL analysis according to three approaches in which we accounted for distinct sets of covariates in the the linear models. We incorporated main effects for sex and SNP geneotype, as well as sex-by-SNP interactions, in all models. First, we implemented linear models regressing the inverse normal transformed gene expression data against three genotype PCs, platform, RIN, and age. Second, we implemented linear models regressing the inverse normal transformed gene expression data against three genotype PCs, platform, RIN, age, and 36 surrogate variables (SVs) identified as described above for our differential expression analysis. Third, we implemented linear models regressing the inverse normal transformed gene expression data against three genotype PCs, platform, RIN, age, and 32 PEER factors. All main text analyses are based on the PEER approach, whereas the other approaches were only considered for our eQTL replication analyses.

In preliminary analyses, we evaluated whether explicitly accounting for population structure using the genetic similarity matrix in a linear mixed model could increase the sensitivity for detecting interaction eQTLs (Listgarten et al., 2010). We implemented the linear mixed models with the 'leave one chromosome out' approach to correct for population structure using `Fast-LMM` (Civelek et al., 2017; Lippert et al., 2011). We compared the results to those of complementary analyses using `Matrix eQTL` to correct for genotype PCs. Our analyses showed that the linear mixed model approach did not enhance sensitivity for detecting interaction eQTLs from the GTEx subcutaneous adipose tissue data set (v6p). Based on this analysis, we completed our study using `Matrix eQTL` (Shabalin, 2012).

Replication analyses: To maximize the sensitivity for replicating associations from the GTEx cohort, in addition to the PEER based eQTL analysis reported in the main text, we also evaluated sex-by-SNP interactions with expression data corrected for hidden factors identified from SVA, as well as correcting only for known covariates. We considered the union of the associations identified with the three approaches for the eQTL replication analysis. We replicated our sex-by-SNP interaction eQTL analysis using data from the STARNET and MGH cohorts (main text Table 1). Subject recruitment and tissue collection in the STARNET data were performed as previously described (Franzén et al., 2016). Briefly, patients with CAD who were eligible for open-thorax surgery at the Department of Cardiac Surgery, Tartu University

Hospital in Estonia as well as control subjects without CAD were enrolled after informed consent. Venous blood was drawn and DNA was isolated for genotyping using the Illumina Infinium assay with the human OmniExpressExome-8v1 bead chip. Data were analyzed using GenomeStudio 2011.1 (Illumina) which produced 951,117 genomic markers. Quality control was performed using `PLINK` (Purcell et al., 2007) and `IMPUTE2` (Howie et al., 2011) was used for genotype imputation to increase the power of analysis. To obtain transcriptome data, biopsies from subcutaneous fat (SF) were obtained and RNA was extracted as described. Cis- regulated expression quantitative trait loci (eQTLs) were identified with `Matrix eQTL` (Shabalin, 2012). Only bi-allelic markers were included and all cis-regulatory SNPs located within 1Mb of the gene were tested using a linear model with a sex-by-SNP interaction term as described above. Interaction eQTLs with minimum nominal p-values < 0.05 per gene were retained for further analysis.

For the replication of the eQTL interaction analysis using the MGH obese subcutaneous adipose tissue data, we implemented the following analyses. We filtered the genotypes for MAF > 0.05 and removed indels. The gene expression normalization methods were described previously (Greenawalt et al., 2011). We performed eQTL analysis using three genotype PCs, age, and pre-operation BMI as covariates, along with sex times SNP genotype as an interaction term, as described above using `Matrix eQTL` (Shabalin, 2012).

We estimated the null replication probability with a permutation test. We specifically addressed the probability of replicating the 2,408 sex-specific eQTLs. We randomly and independently permuted all of the association p-values and and effect sizes 1000 times. For each of the 1000 permutations, we determined the number of replicated associations ($P < 0.05$, identical effect direction). The average null replication rate was 2.5% (range 1.66-3.74%).

Determining linkage disequilibrium (LD): We generated the LD relationships for the unfiltered GTEx genotype data using version 1.9 of `PLINK` (Purcell et al., 2007). We evaluated LD within 2 Mb and excluded variant pairs with more than 999,999 intervening SNPs. We focused on SNP pairs with LD $r^2 > 0.8$ for our analyses.

Overlapping eQTLs with genome-wide association study (GWAS) variants: We download GWAS summary statistics, for an expansive range of published disease or trait association analyses, from the `GWAS catalog` in December of 2019 (`https://www.ebi.ac.uk/gwas/downloads`) (Buniello et al., 2019). We filtered the `GWAS catalog` data for associations with genome-wide significance ($P < 5 \times 10^{-8}$). To determine whether sex-specific eQTL SNPs matched sex-specific associations with body fat distribution, we considered the results from two recent GWAS studies (Rask-Andersen et al., 2019; Pulit et al., 2019). The genome-wide significant sex-specific associations from Rask-Andersen et al. (2019) were obtained from their Table 2 (Bonferroni-corrected p-value $< 3.57 \times 10^{-4} = 0.05/n$ where n is the number of tests). The genome-wide significant sex-specific associations from Pulit et al. (2019) were obtained from their Supplementary Table 8 (Bonferroni-corrected p-value $< 3.3 \times 10^{-5} = 0.05/n$ where n is the number of tests).

ChromHMM analysis: We overlapped the the sex-specific eQTL SNPs with genomic annotations identified with `ChromHMM` (Ernst and Kellis, 2012). The genomic annotations were identified from Epigenetics Roadmap ChiP-seq data from adipose-derived cultured mesenchymal stem cells (pre-adipocytes, epigenome ID E025) and mesenchymal stem cell-derived cultured adipocytes (epigenome ID E023) (Roadmap Epigenomics Consortium et al., 2015). BED coordinates for the genomic annotations were downloaded from `https://egg2.wustl.edu/roadmap/data/byFileType/chromhmmSegmentations/ChmmModels/coreMarks/jointModel/final/`. The `ChromHMM` data were obtained from the 15-state model based on five chromatin marks (H3K4me3, H3K4me1, H3K36me3, H3K27me3 and H3K9me3). We aggregated state descriptions as follows (main text Fig 3D): TSS (transcription start site) includes "Active TSS", "Flanking Active TSS", and "Bivalent/Poised TSS" (states 1,2,10); transcribed includes "Transcr. at gene 5' and 3'", "Strong transcription", and "Weak transcription" (states 3,4,5);

enhancer includes "Genic enhancers", "Enhancers", and "Bivalent Enhancer" (states 6,7,12); repressed includes "Heterochromatin", "Repressed PolyComb", and "Weak Repressed PolyComb" (states 9,13,14); quiescent includes "Quiescent/Low" (state 15); other includes "ZNF genes & repeats" and "Flanking Bivalent TSS/Enh" (states 8,11).

Chromatin contact analysis of HiC data: We evaluated promoter-capture (pc) Hi-C data from human pre-adipocytes (Pan et al., 2018). We overlapped the pcHi-C bait coordinates with `GENCODE` gene annotations (Frankish et al., 2019). In a strand specific manner, we defined ranges for transcription start sites (TSSs) of annotated genes by taking the coordinates encompassing all first exons for a given gene. After annotating the pcHi-C bait regions with the TSS regions from `GENCODE`, we overlapped the pcHi-C bait coordinates with sex-specific eQTL genes and we overlapped the pcHi-C capture coordinates with sex-specific eQTL SNPs. For each eQTL locus, we considered a range encompassing SNPs in linkage (LD $r^2 > 0.8$). We performed a permutation test to estimate the probability of intersecting a random set of eQTL associations, irrespective of the association p-value, with the pcHi-C coordinates. For each of 1000 permutations, we randomly selected 2,408 associations. For each association, we considered a 60 kb interval centered on the lead SNP to account for linkage when overlapping the locus with the pcHi-C targets (Reich et al., 2001). The average percentage of random associations for which both the eQTL SNP and gene matched the pcHi-C capture and bait coordinates, respectively, was 1.6% (range: 1.0-2.5%).

Analysis of gene expression dynamics during adipogenesis

We download the adipogenesis timeseries gene expression data from `GEO` (main text Table 1). We considered human SGBS data, human abdominal pre-adipocyte data, and murine 3T3-L1 data. The human SGBS microarray data (Nassiri et al., 2016) and the human adipose-derived stromal cell (ASC) microarray data (Ambele et al., 2016) were evaluated for dynamic expression by fitting linear models with respect to time and applying the likelihood ratio test (LRT) to compare the time-dependent models to time-independent null models (intercept only). The 3T3-L1 murine RNA-seq data were matched for orthologs of the human genes of interest using the `biomaRt` R package and the LRT was implemented using `DESeq2` after normalizing the data based on sequencing depth-related size factors (Love et al., 2014). For all three data sets, we estimated the transcriptome-wide expression percentiles for genes of interest in mature adipocytes at the time point of terminal differentiation.

Supplemental Results

Normalization constrains fold change assessment

Here we show that, given an inverse-normal transform, the maximal fold change is constrained by the sample size (n) and relative numbers of females and males in the sample (n_f, n_m). Consider a case in which we apply the inverse-normal transformation for a specific gene:

$$e^i_{norm} = \Phi^{-1}\left(\frac{r_i}{n+1}\right) \qquad (eq1)$$

where e^i_{norm} is the normalized expression level of a given gene for the ith sample, r_i is the rank for the ith sample, $n = n_f + n_m$ is the number of samples, and Φ refers to the cumulative distribution function of the standard normal distribution, $\mathcal{N}(0,1)$. Then e_{norm} will be normally distributed with the following probability density and cumulative distribution functions

$$\phi(e^i_{norm}) = \frac{1}{\sqrt{2\pi}} exp\big(-\frac{1}{2}(e^i_{norm})^2\big) \qquad (eq2)$$

$$\Phi(e^i_{norm}) = \frac{1}{2}\left[1 + erf\Big(\frac{e^i_{norm}}{2}\Big)\right] \qquad (eq3)$$

such that $erf(.)$ is the error function. For illustrative purposes, consider a gene for which expression is greater in females. According to the inverse-normal transform, the greatest possible fold change will be achieved when the normalized expression values for all of the females are greater than the highest normalized expression value over all of the males ($\min(e_f) > \max(e_m)$, $e_f \in \mathbb{R}^{n_f}$, $e_m \in \mathbb{R}^{n_m}$). That is, the ranks of the expression values for the males are $\{1, 2, ..., n_m\}$ and the ranks for the females are $\{n_m + 1, n_m + 2, ..., n_m + n_f\}$. Assuming the data are subjected to a standard differential expression analysis, and are therefore in the 'log space', the fold change is defined as follows (Ritchie et al., 2015):

$$fc = 2^{mean(e_f) - mean(e_m)} = 2^{\mu_f - \mu_m} \qquad (eq4)$$

Correspondingly, the log fold change is defined as $\mu_f - \mu_m$. Under the stated assumptions, the respective expression means are defined as follows (see ($eq2$)), considering the truncated normal distribution (Foulley, 2000):

$$\mu_m = E(e_m | -\infty < e_m < \Phi^{-1}(N_m)) = \frac{\phi(-\infty) - \phi(\Phi^{-1}(N_m))}{\Phi(\Phi^{-1}(N_m)) - \Phi(-\infty)} \qquad (eq5)$$

$$\mu_f = E(e_f | \Phi^{-1}(N_m) < e_f < \infty) = \frac{\phi(\Phi^{-1}(N_m)) - \phi(\infty)}{\Phi(\infty) - \Phi(\Phi^{-1}(N_m))} \qquad (eq6)$$

where $N_m = r_m/(n+1)$ such that r_m refers to a particular rank related to the fraction of males in the sample. Then the log fold change is as follows:

$$\mu_f - \mu_m = \frac{\phi(\Phi^{-1}(N_m))}{\Phi(\Phi^{-1}(N_m))(1 - \Phi(\Phi^{-1}(N_m)))} = \frac{\frac{1}{\sqrt{2\pi}} exp\big(-\frac{1}{2}(-\sqrt{2} erf^{-1}(1 - 2N_m))^2\big)}{N_m(1 - N_m)} \qquad (eq7)$$

assuming that $\Phi \circ \Phi^{-1}(x) = x$. As shown in Supplemental Fig S2 (see below), the relation given by ($eq7$) is relatively flat over a range for the fraction of males in the sample. Substantial fold change differences are observed as the entire sample approaches either all males or all females (Supplemental Fig S2A). However, an ideal sampling procedure will ensure roughly equal numbers of males and females and a large sample

size, in which case $r_m/(n+1)$ approaches 0.5 (i.e., $N_m \to 0.5$). Therefore, for an experimental design with ideal sampling, the upper bound on the log fold change is as follows (given that $erf^{-1}(0) = 0$):

$$\lim_{N_m \to 0.5} \mu_f - \mu_m = \frac{4}{\sqrt{2\pi}} \sim 1.6 \qquad (eq8)$$

We simulated normally distributed gene expression with random samples from $\mathcal{N}(0,1)$ and varied the total sample size and fraction of males. To evaluate the maximal fold change, we assumed that the highest male expression level was lower than the lowest female expression level, as described above. We compared the observed data to the theoretical expectations from ($eq7$) and ($eq8$) (Supplemental Fig S2). The results show that the largest fold changes are observed when the samples are either nearly all males or nearly all females (Supplemental Fig S2A). The optimal upper bound for evenly sampled data is given by ($eq8$), which is the limit of ($eq7$) as the sample size goes to infinity and the fraction of males goes to 50%. To approximate the upper bound on the fold change, we varied the sample size between 100 and 100,000. For each element in the sample size range, we varied the fraction of males and computed the maximal observed and expected log fold change. This analysis shows that, for inverse normal transformed data subjected to a differential expression analysis, the predicted upper bound on the log fold change is approximately four, whereas the optimal upper bound is approximately 1.6 (Supplemental Fig S2B). Importantly, this analysis highlights the impact of normalization in constraining the observable fold changes in a differential expression analyses. If a data set is strictly normal ($\mathcal{N}(0,1)$), with identical male and female sample sizes, it is not possible to observe a log fold change above the upper bound given by ($eq8$). In general, caution should be exercised in comparing fold changes from data sets for which normalization approaches are distinct.

GSEA of race-stratified GTEx data (multi-ethnic cohort)

Our results showed that the enrichments for fatty acid metabolism and KLF14 targets from African American AAGMEx cohort were negative, whereas those for GTEx and deCODE cohorts were positive (main text Fig 2B). To address whether this difference in directionality could be attributed to race, we stratified the multi-ethnic American GTEx cohort into African American and non-African American subsets and implemented GSEA. The results from the race-stratified multi-ethnic American GTEx cohort analysis did not match those of the African American AAGMEx cohort (Supplemental Fig S7). To determine whether a deficit in statistical power could account for the discrepancy between the African American cohort and the other two cohorts, we evaluated the fold changes correlations amongst cohorts for gene sets underlying the enriched annotations (see main text Fig 2C).

Sex-specific eQTL replication analysis

To determine the generality of the sex-specific eQTLs identified through our analyses, we replicated these analyses using subcutaneous gene expression data from two additional cohorts: the STARNET healthy cohort (Franzén et al., 2016) and the obese MGH cohort from the US (Greenawalt et al., 2011). Our replication criteria were $P < 0.05$ and consistent directionality for the interaction effect size. For the STARNET cohort, we observed 50 replicated loci out of 2,220 complementary associations (2.3%; P=0.75, permutation test). For the MGH cohort, we observed 64 replicated loci out of 1,538 complementary associations (4.2%; P=0, permutation test). Replication data are provided in the Supplemental Table S8). The low rate of replication could be due to phenotypic differences in the cohorts (e.g., the MGH cohort consisted of obese patients), geographic/ethnic differences (e.g., the STARNET cohort was from Estonia), or differences related to the nuances of the data processing.

Overlap of sex-specific eQTLs with human GWAS variants

We first considered recent sex stratified GWASs of adipose tissue distribution (Rask-Andersen et al., 2019; Pulit et al., 2019). We did not find any overlaps between adipose tissue sex-specific eQTLs and genome-wide significant GWAS loci ($p < 5 \times 10^{-8}$, LD $r^2 > 0.8$). We next overlapped the sex-specific eQTL SNPs with disease- or trait-associated SNPs identified through human GWAS analyses available in the GWAS catalog (Buniello et al., 2019). We performed an analysis to determine whether sex-specific eQTLs could be colocalized with the GWAS traits, however, no such evidence was observed (maximal probability of single variant colocalization = 0.65). This is likely related to the fact that the GWAS catalog only contains SNPs with $P < 9 \times 10^{-6}$. As a result, there were $\leq$8 variants for a given eQTL locus (LD $r^2 > 0.6$) and GWAS trait combination, therefore underpowering the colocalization analysis and preventing the application of other related approaches such as summary-based Mendelian Randomization analysis (Civelek et al., 2017).

Overlapping sex-specific eQTLs with chromatin contacts

We evaluated whether sex-specific eQTLs, as well as SNPs in high LD ($r^2 > 0.8$), overlapped with adipose tissue chromatin contacts inferred from promoter-capture (pc) Hi-C data obtained from human pre-adipocytes (Pan et al., 2018). We identified chromatin contacts between eQTL SNPs and eQTL genes for 39 out of 2,408 associations (1.6%, $P = 0.58$, permutation test). None of the 162 sex-biased genes were identified in this analysis. The absence of a substantial overlap between the sex-specific eQTLs and the chromatin contacts identified in cultured pre-adipocytes could be due to differences between *in vitro* and *in vivo* conditions, differences between pre-adipocytes and adipocytes, or differences between the eQTL analysis population and the single donor in the pcHi-C study.

Non-sex-specific eQTL overlap with open chromatin regions

We downloaded the non-sex-specific eQTL data from the GTEx portal `https://www.gtexportal.org/home/`. As with our sex-specific eQTL analysis, we considered the lead SNPs from associations with $P < 1 \times 10^{-4}$. We overlapped all unique SNPs with four sets of open chromatin peaks: (1) pre-adipocyte peaks, (2) adipocyte peaks, (3) the union of pre-adipocyte, adipocyte, and adipose tissue peaks, and (4) the intersection of pre-adipocyte, adipocyte, and adipose tissue peaks. Out of 14,906 SNPs, 6% were in the intersection of all peak classes, 14% were in pre-adipocyte peaks, 17% were in adipocyte peaks, and 18% were in the union or all peak classes.

Analysis of sex-specific eQTL SNP enrichment in TF binding motifs within open chromatin peaks

To determine whether sex-specific eQTL SNPs were enriched in TF binding motifs within open chromatin peaks, we quantified the counts of loci overlapping TF binding motifs and open chromatin regions from the four sets of peaks. We observed a trend of association between sex-specific eQTL SNPs within TF binding motifs and open chromatin peaks. However, the results were not statistically significant (all odds ratios > 1.07, FDR > 0.55, Fisher's exact test). This finding could be related to the fact that the presence of consensus TF motif does not necessarily entail functional binding, therefore highlighting the importance of evaluating functional data when investigating associations with genomic features. These results could also occur if the mechanisms underlying sex-specific allelic effects on gene expression are predominantly related to allelic effects on TF binding in proximity, but not directly overlapping, the associated SNPs

(Deplancke et al., 2016). Furthermore, these results could be related to numerous differences between the ATAC-seq samples and the samples used for the eQTL analysis. Nevertheless, 0.7%, 3.5%, 4.6%, 5.2%, of the sex-specific eQTL loci overlapped TF binding motifs that were within intersect peaks, pre-adipocyte peaks, adipocyte peaks, and union peaks, respectively. These analyses identified functionally relevant loci for which sex-specific allelic effects on gene expression could be explained by TF binding to consensus motifs within open chromatin regions.

Our findings presented thus far reveal loci for which binding of differentially expressed TFs could potentially explain sex-specific eQTLs, but we also found that sex-specific loci overlapping TF binding motifs were not significantly enriched in open chromatin regions. To address this potential discrepancy, we integrated and further examined the aforementioned data. First, we identified all sex-specific eQTL loci that were both overlapping a TF binding motif and within open chromatin regions from the union of pre-adipocyte peaks, adipocyte peaks, and adipose tissue peaks. The overlapping TF motifs corresponded to TFs implicated in adipogenesis, as described above (e.g., PPARG, KLF5, EGR1, EGR2, SREBF2; Supplemental Table S9). We identified five open chromatin loci overlapping PPARG motifs. For example, an open chromatin locus associated with *BRD4* expression overlapped a consensus motif for the PPARG-RXRA dimer (main text Fig 4F,G). These results support the functional relevance of sex-specific eQTL overlapping putative TFBSs in open chromatin regions.

Gene expression dynamics in human and mouse adipogenesis

For these analyses we focused on *FADS1*, *MAP1B*, *HSPA12A*, *CLIC6*, *MMD*, and *PDZD2* (along with the respective murine orthologs). We first evaluated gene expression in the SGBS human adipocyte cell line (Nassiri et al., 2016). In differentiated SGBS adipocytes, the six aforementioned genes were within the upper expression quartiles (percentile > 0.5). To determine whether the expression of these genes varied throughout the process of adipocyte differentiation, we analyzed adipogenesis time-series data in SGBS cells (Nassiri et al., 2016). We evaluated the dynamics of gene expression by fitting linear models to the gene expression profiles, with and without associations with differentiation time, and applying a Likelihood Ratio Test (LRT) to compare the models. Our analysis was consistent with the temporal dependences of *FADS1*, *MAP1B*, *HSPA12A*, *CLIC6*, *MMD*, and *PDZD2* during adipogenesis (FDR $\leq 2.7 \times 10^{-4}$, main text Fig 7).

To further evaluate whether *FADS1*, *MAP1B*, *HSPA12A*, *CLIC6*, *MMD*, and *PDZD2* are expressed in adipocytes acutely isolated from human subcutaneous adipose tissue, we evaluated time-series gene expression data from adipogenesis experiments with human adipose-derived stromal cells during adipocyte differentiation (Ambele et al., 2016). These data included samples from three females and one male, hence it was not possible to evaluate sex-differences due to statistical power limitations associated with the low sample sizes. Our analyses were generally consistent with dynamic expression during adipogenesis (FDR ≤ 0.052, LRT, Fig 7). As observed for SGBS cells, the genes of interest were largely within the upper expression quartiles. These data are consistent with the robust functional expression of differentially expressed sex-specific eQTL genes in human subcutaneous adipocytes. The pronounced augmentation of *FADS1* early in adipogenesis in consistent with a role of the FADS1 enzyme in coordinating the differentiation process.

To evaluate the conservation of *FADS1*, *MAP1B*, *HSPA12A*, *CLIC6*, *MMD*, and *PDZD2* expression dynamics in murine adipogenesis, we examined time-series adipogenesis data from 3T3-L1 cells (Siersbæk et al., 2017). Consistent with the human adipocyte data, our analysis revealed that *Fads1* and *Map1b* were in the upper expression quartiles for mature adipocytes, and showed dynamic expression during adipogenesis (FDR $\leq 5.6 \times 10^{-9}$, LRT; Fig 7). However, the *Fads1* dynamics followed a distinct kinetic profile as compared to the rapid *FADS1* response observed for human adipocytes.

Supplemental Discussion

Sex differences related to mitochondrial function

Data from both mice and humans are consistent with elevated mitochondrial oxidative metabolism in females (Keuper et al., 2019; Norheim et al., 2019; Bayindir-Buchhalter et al., 2018; Silaidos et al., 2018; Gaignard et al., 2018; Vijay et al., 2015; Rodriguez-Cuenca et al., 2002). It was previously reported that sex differences were not observed in measures of oxygen consumption rate from human adipocytes, however, it does not appear that this study was adequately powered to for such an analysis (N = 15, (Yin et al., 2014)). Another study reported sex differences in oxidative metabolism in human pre-adipocytes, but not mature adipocytes, from obese donors (N = 20, Keuper et al. (2019)). Again, these findings could be due to either power limitations or the fact that the donors were obese. Further work is needed to establish whether gene expression sex differences propagate to sex differences in the oxidative metabolism of adipose tissues.

Sex differences related to adipogenesis

Previous reports have documented sex differences in adipogenesis (Blouin et al., 2010), and sex hormones are known regulators of adipocyte differentiation (Blouin et al., 2010; Gupta et al., 2008; Singh et al.). Other studies have shown the absence of sex differences in adipogenesis (Contreras et al., 2016; Tchoukalova et al., 2010). Methodological details regarding pre-adipocyte isolation and the quantification of adipogenesis may be critical to the interpretation of the existing results. In general, adipogenesis is a process that involves the proliferation followed by the differentiation of progenitor stem cells that are committed to the adipocyte lineage (i.e., pre-adipocytes, Ghaben and Scherer (2019)). Human and rat pre-adipocytes from females showed enhanced proliferation following estradiol treatment in comparison to those from males (Anderson et al., 2001; Dieudonne et al., 2000). Dihydrotestosterone was shown to inhibit adipocyte differentiation of human male pre-adipocytes (Gupta et al., 2008). Testosterone and dihydrotestosterone inhibited adipocyte differentiation in male murine 3T3-L1 cells (Singh et al.). A related study showed that androgens inhibited human adipocyte differentiation, with an elevated effect in females as compared to males (Blouin et al., 2010).

Results from measurements of radioactive carbon isotope incorporation into subcutaneous adipose tissue DNA supported the conclusion that adipogenesis occurs in human adults to maintain a constant cell number with an 8% cell turnover per year (Spalding et al., 2008). However, it should be noted that this conclusion was derived from analyses of partial differential equation models of the data. Thus, limitations related to the model assumptions, specification, and fit may influence this interpretation (Bernard et al., 2010). Further, the model analysis was based on abdominal adipose tissue (Spalding et al., 2008), whereas evidence consistent with sex differences in human adipogenesis *in vivo* was shown to be more prominent in the femoral subcutaneous depot (Tchoukalova et al., 2010). Available *in vitro* data, based on the assessment of *PPARG* expression in differentiated pre-adipocyte cultures from abdominal subcutaneous adipose tissue biopsies, do not support elevated adipogenesis in females (Tchoukalova et al., 2010). These *in vitro* results rendered the *in vivo* findings ambiguous. Irrespective of sex, multiple view points exist as to whether adipogenesis contributes to adipose tissue mass in adult humans, with contributions to health and disease (Vishvanath and Gupta, 2019), or whether adipocyte numbers are relatively fixed (Spalding et al., 2008), and there are a number of important caveats regarding the existing data (Arner and Spalding, 2010).

Study limitations

This study has several limitations that represent opportunities for further investigation. A general caveat of adipose tissue-scale analyses of sex differences is that the differences could be due to sex-biased expression in adipocytes, sex-biased expression in non-adipocytes (e.g., adipose tissue macrophages or vascular cells (Rosen and Spiegelman, 2014)), and/or sex-differences in the proportions of cell types across which expression variation is present (see Khramtsova et al. (2019)). However, it has been shown that gene expression profiles from human adipose tissue largely reflect adipocyte expression patterns, such that subject-to-subject differences substantially exceed tissue-to-adipocyte differences (see Fig S3 in Hu et al. (2019)). Another important caveat is that we used a permissive p-value cutoff for our sex-specific eQTL analysis (i.e., 1×10^{-4}). Our rationale was that we could apply permissive eQTL discovery criteria and subsequently impose rigorous statistical criteria in downstream analysis. That is, we applied a sensitivity filter followed by specificity filters. Importantly, we implemented interaction models for our eQTL analysis, which are preferable for detecting sex-by-genotype interactions (Gilks et al., 2014), at the cost of reduced power for detecting interactions (Brookes et al., 2004). Nevertheless, we acknowledge that our choice in significance threshold led to a greater extent of interaction eQTL discovery as compared to other studies (Yao et al., 2014). Another approach would be to assess main effects for genotype in sex-stratified analyses (Norheim et al., 2019), however, such approaches have reduced reliability (Brookes et al., 2004). As an alternative to an unbiased genome-wide eQTL analysis, one could perform feature selection prior to association mapping (Ho et al., 2019), to limit the false discovery burden. For instance, the analysis could be performed only for SNPs within open chromatin peaks or transcription factor binding sites. Such an approach would be biologically motivated by studies demonstrating that veritable cis-regulatory variants are enriched within open chromatin regions (DNAse hypersensitivity sites), active promoters/enhancers (H3k4me3, H3k27ac ChIP-seq) and transcription factor binding sites (ChiP-seq) (Tewhey et al., 2016). In general, our analyses were designed to prioritize specificity over sensitivity. We combined data from a variety of resources (e.g., distinct ethnicities and cell line data). Focused comparisons (e.g., between ethnicities) would not be justifiable due to the absence of systematic data collection and initial processing procedures. Nevertheless, the findings we report here are robust to a plethora of potentially confounding factors. Therefore, we consider the sensitivity limitation of our study to be a positive attribute in the form of enhanced specificity and robustness. To resolve many limitations of our study, analyses of adipocytes from a large cohort of human donors could be advantageous.

Functions of *FADS1*, *MAP1B*, *HSPA12A*, *CLIC6*, *MMD*, and *PDZD2*

Fatty Acid Desaturase 1 (FADS1) is a fatty acid metabolism enzyme involved in the metabolism of poly-unsaturated fatty acids. FADS1 activity produces arachidonic acid and eicosapentaenoic acid. FADS1 was previously implicated in sex-differences in general metabolism, as well as adipose tissue sex-differences (Guo et al., 2017). FADS1 is a well known regulator of adipose function (Gromovsky et al., 2018; Guo et al., 2017; Viguerie et al., 2012), adipocyte biology (Gromovsky et al., 2018; Zhang et al., 2016; Ralston et al., 2015), and mitochondrial function (Gromovsky et al., 2018). The Microtubule Associated Protein 1B (MAP1B) is involved in transport along microtubles. This gene has been implicated in adipose tissue function in an unbiased gene expression analysis (Dahlman et al., 2010), and was also implicated in mitochondrial function (Jiménez-Mateos et al., 2006). Heat Shock Protein Family A (Hsp70) Member 12A (HSPA12A) is a regulator of the heat shock pathway. This gene is known to contribute to adipocyte biology and adipogenesis, in which interactions with PPARG regulate both differentiation and diet induced obesity (Zhang et al., 2019). In general, HSPA12A is a well documented contributor to adipose biology (Cheng et al., 2019; Tareen et al., 2018; Perfilyev et al., 2017). Chloride Intracellular Channel 6 (CLIC6) is a membrane chloride ion transporter that has been implicated in adipose tissue (Elbein et al., 2011; Lê et al., 2011) and adipocyte biology (Min et al., 2019). Monocyte To Macrophage Differentiation

Associated (MMD) exhibits sex-biased expression in human skeletal muscle (Maher et al., 2009), and has been identified in unbiased gene expression analyses of human adipose tissue (Dahlman et al., 2005). PDZ Domain Containing 2 (PDZD2) is known to be involved in inflammatory signaling and has been identified as a sex-biased gene in murine studies of rheumatoid arthritis (Kudryavtseva et al., 2012). This gene has also been implicated in adipose tissue biology (Chen et al., 2018; Tareen et al., 2018), adipogenesis (Gérard et al., 2019), adipocyte biology (Min et al., 2019; Lo et al., 2013), and mitochondrial function (Arroyo et al., 2016).

Supplemental Code

The supplemental codes are included in the online Supplemental Material as .R and .sh files for respective analyses in R and in the command line.

Supplemental Tables

The supplemental tables are included in the online Supplemental Material as tab-delimited text files for either analysis or inspection in the spreadsheet format. Each supplemental table file has a header with a table legend.

Supplemental Figures

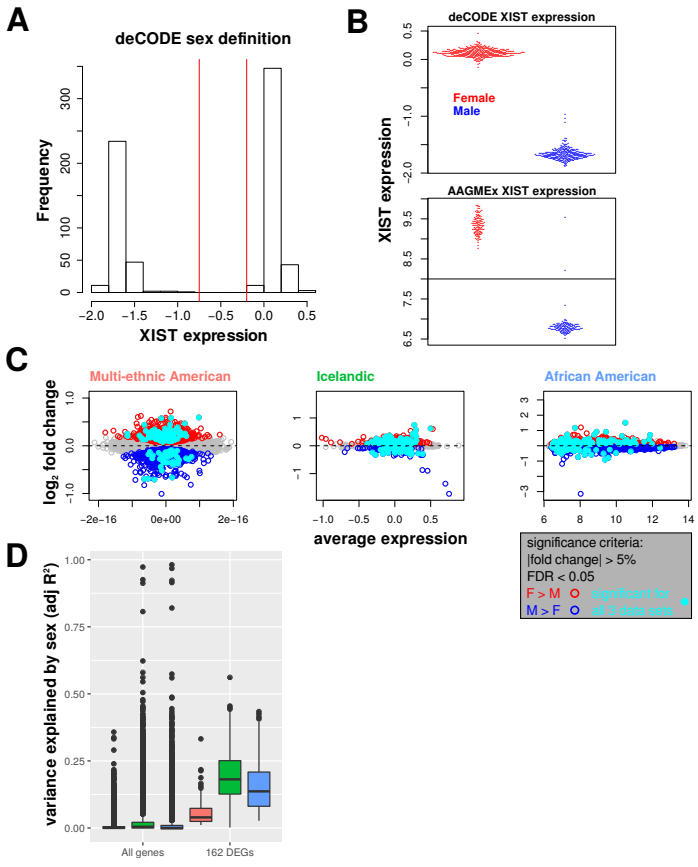

Figure S1: Sex annotation and differential expression analysis. (A) The deCODE *XIST* expression distribution was considered for defining sex annotation. Samples with *XIST* expression levels below the first vertical red line were annotated as males. Samples with *XIST* expression levels above the second vertical red line were annotated as females. **(B)** Annotated sex was consistent with low/negligible *XIST* expression for males and relatively high *XIST* expression for females from the deCODE cohort. Annotated sex was generally consistent with low/negligible *XIST* expression for males and relatively high *XIST* expression for females from the AAGMEx cohort. Two male subjects with *XIST* expression levels above the horizontal black line were removed from the AAGMEx analysis. **(C)** Gene expression log2 fold changes with respect to sex are plotted as a function of average expression level for the three cohorts. **(D)** To assess the gene expression variance explained by sex, we fitted the normalized gene expression profiles, used for the differential expression analysis, with linear models as functions of sex. The proportion of variance explained by sex is greater on average for the differentially expressed genes as compared to the averages over all genes. We performed a permutation test the evaluate the significance of the average variance explained by randomly selecting 162 genes from each data set over 10,000 iterations. For each of the three data sets, there was a zero probability of identifying an average variance explained as high as that observed for the mean variance explained for the 162 differentially expressed genes from the respective data set.

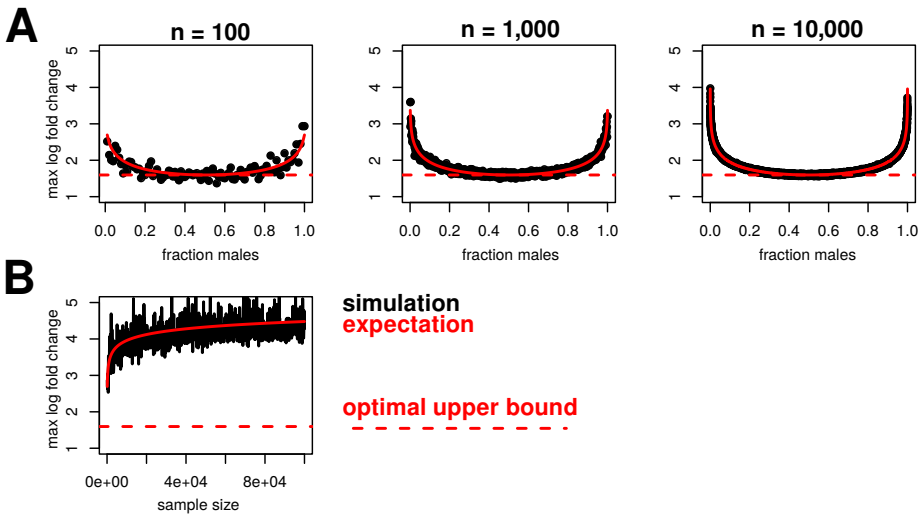

Figure S2: The inverse normal transform constrains fold change estimation in differential expression analysis. (A) The log fold change is convex with respect to the fraction of males. **(B)** The maximal expected fold change shows an asymptotic limit at approximately four for sample sizes up to 10,000. The simulated data were generated from random normal distributions and the expectation traces were generated from equation 7. The optimal upper bound was based on equation 8. See Supplemental Results for further details.

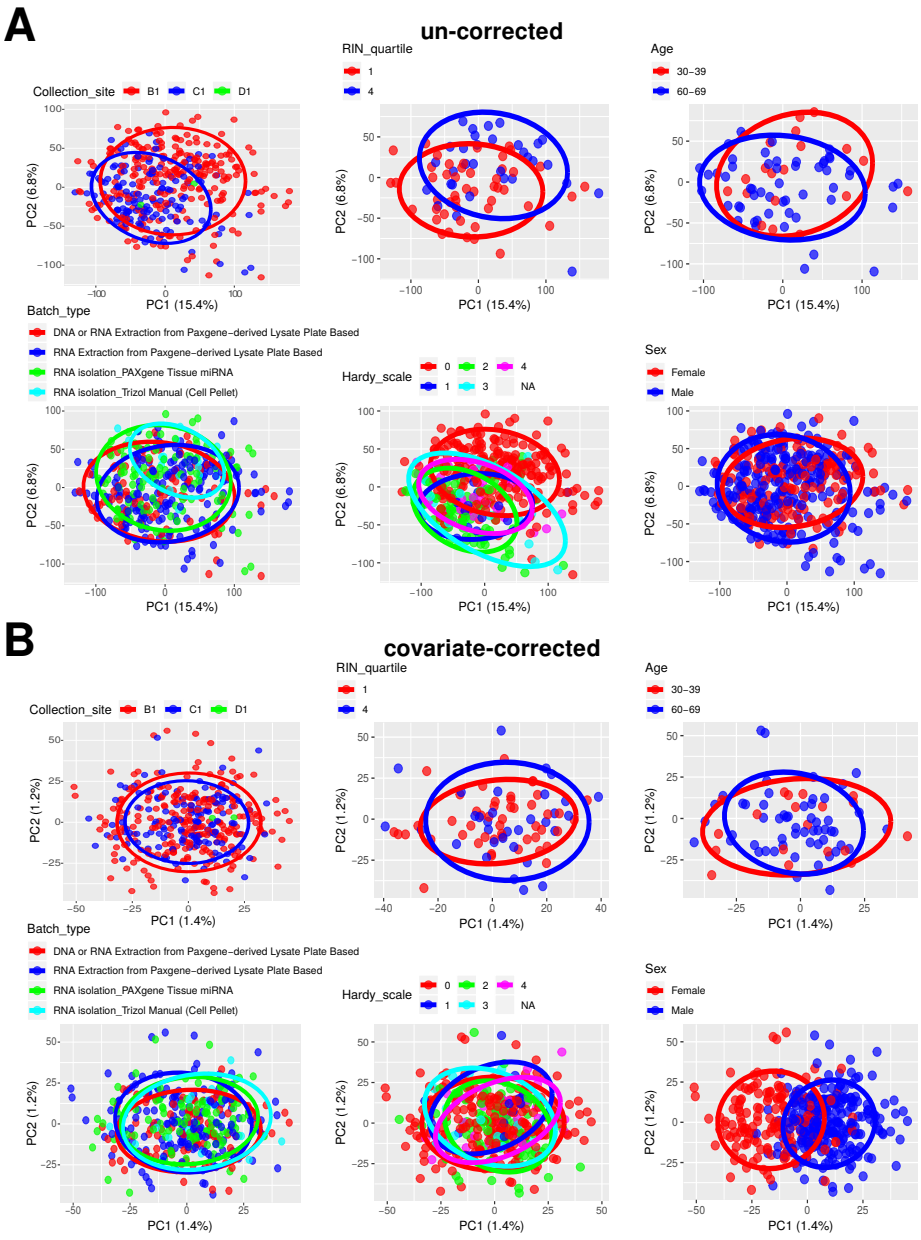

Figure S3: Correction for surrogate variables highlights sex differences in gene expression. (A) Principal component plots illustrate the systematic effects of collection site (top left), RNA integrity number (RIN, top middle), age (top right), batch type (bottom left), Hardy scale representing death circumstances (bottom middle), and sex (bottom right) on gene expression. **(B)** Principal component plots complementary to those in **(A)** are shown for PC projections of the residuals obtained after adjusting the data for age, RIN, platform, and the 36 latent factors from surrogate variable analysis (SVA). Note that the visible effects of collection site, RIN, age, batch type, and Hardy scale are not apparent following covariate correction. In contrast, the sex differences are accentuated following the covariate adjustment (compare bottom right of **(B)** with the bottom right of **(A)**). Ellipses denote 75% confidence intervals for bivariate normally distributed data.

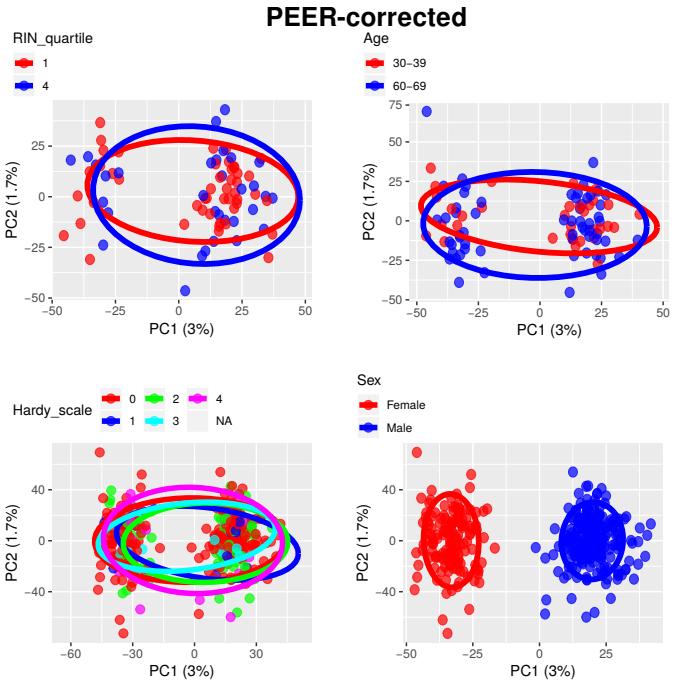

Figure S4: Correction for PEER factors highlights sex differences in gene expression. Principal component plots are shown for PC projections of the residuals obtained after adjusting the data for age, RIN, platform, and the 32 latent factors from the PEER analysis. Note that the visible effects of RIN, age, and Hardy scale are not apparent following covariate correction. In contrast, the sex differences are accentuated by the adjustment for PEER factors (compare with panel **(A)** of Supplemental Fig S3). Ellipses denote 75% confidence intervals for bivariate normally distributed data.

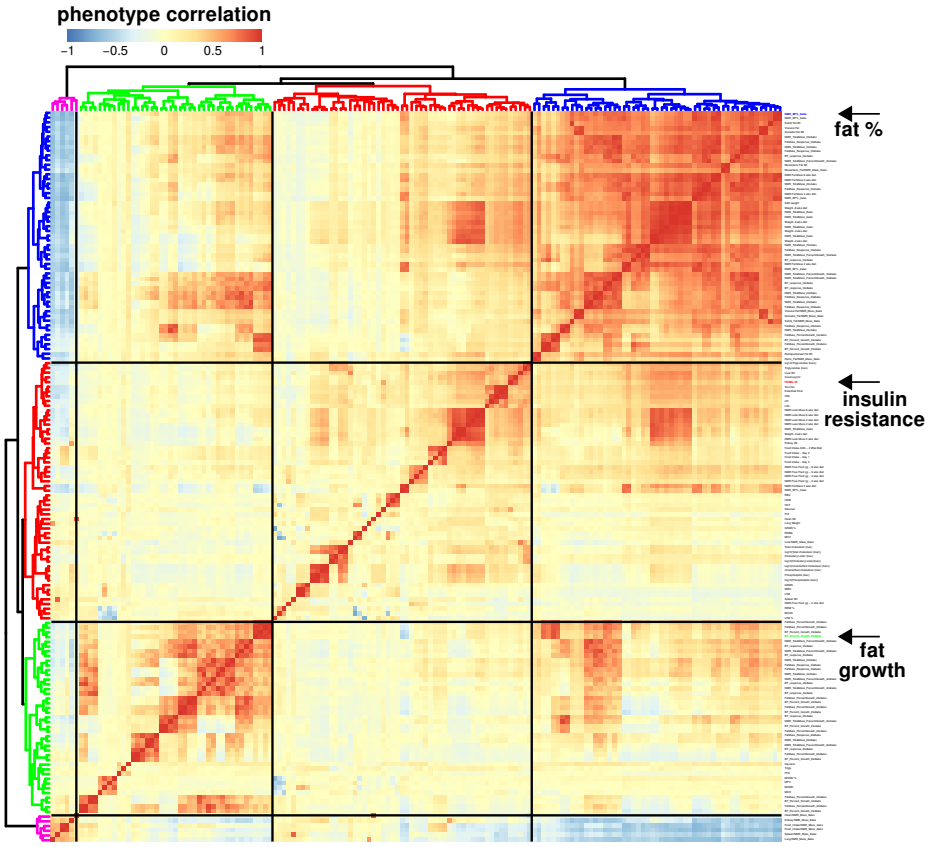

Figure S5: Phenotype correlation analysis to select metabolic traits for the fold change correlation analysis in mice. We clustered the Pearson correlation matrix based on Euclidean distance. The analysis revealed three prominent clusters. We inspected the cluster constituents and selected body fat percentage, insulin resistance, and body fat growth as representative phenotypes.

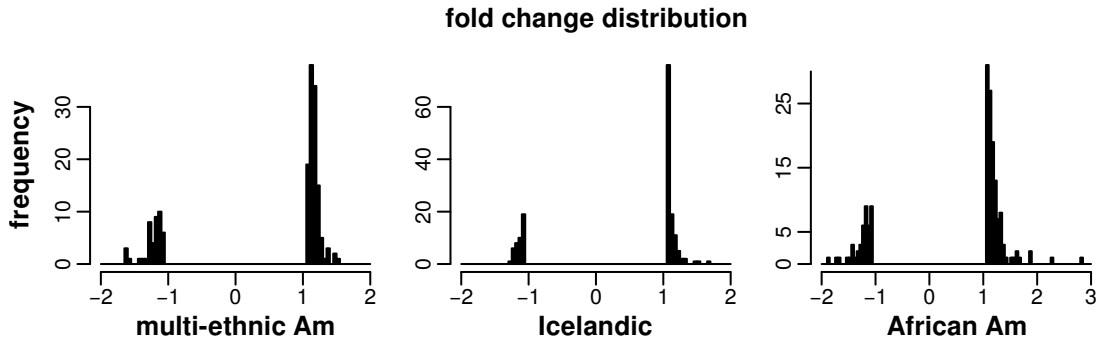

Figure S6: Fold change distributions for differentially expressed genes. We found that 162 genes were differentially expressed in subcutaneous adipose tissue, with consistent directionality, across three geographically and ethnically diverse human cohorts (|fold change| > 1.05, FDR < 0.05). For symmetry with respect to fold change directionality, we plot negative log fold changes as $-1/2^{log_2(fc)}$ (e.g., for log_2(fc) = -2, fc $= -1/2^{-2} =$ -4 for symmetry with $2^2 = 4$).

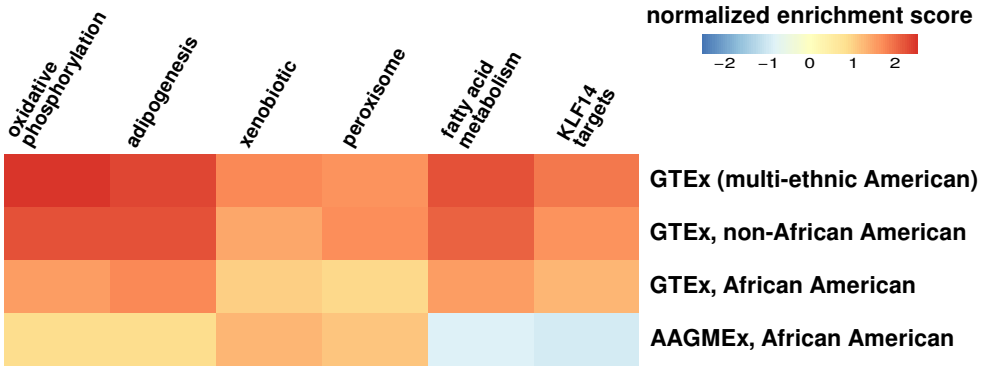

Figure S7: Race-stratified gene set enrichment analysis (GSEA) of the GTEx data. We separated the subcutaneous adipose tissue GTEx data into African American (n=71; 25 females, 46 males) and non-African American samples (n=510; 169 females, 341 males). The GSEA results show that the effect size directionality differences between the multi-ethnic GTEx cohort and the AAGMEx cohort, observed for fatty acid metabolism and KLF14 targets, are maintained when the GTEx data are stratified by race. This suggests that the difference between the GTEx and AAGMEx results is not attributable to race.

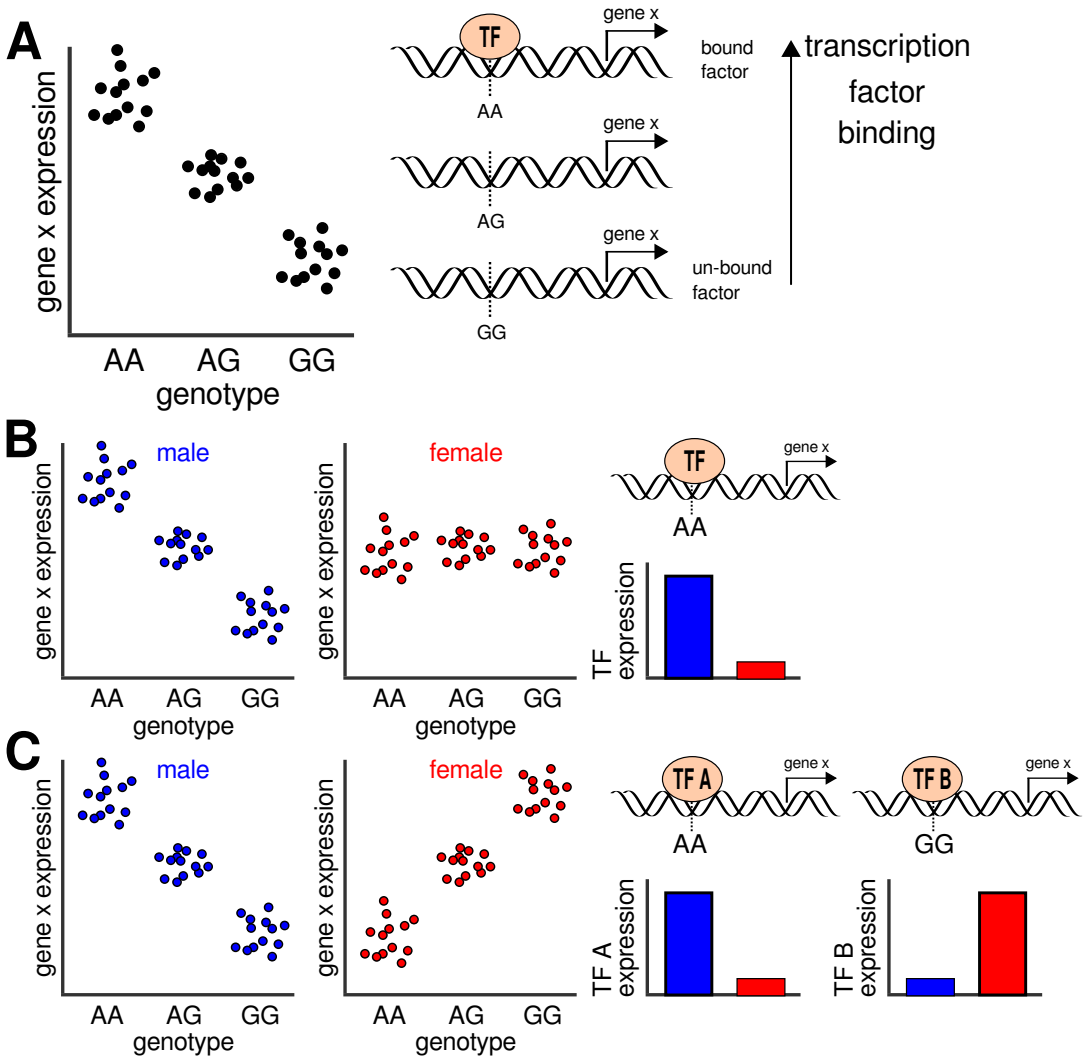

Figure S8: Mechanistic hypotheses for sex-specific eQTLs. (A) We considered cases in which eQTL associations are directly related to transcription factor (TF) binding at a single regulatory SNP. According to this model, if a TF is an activator of expression, its allele-specific binding should be associated with elevated expression. In this example, TF affinity and gene expression are relatively elevated in individuals homozygous for the A allele. **(B)** We hypothesize that a sex-specific eQTL effect, with a sex-specific effect observed only in males, can be explained by male-specific expression and enhanced binding of an activator TF to the allele associated with elevated expression. **(C)** We hypothesize that a sex-specific eQTL, with a sex-specific directionality, can be explained by instances in which the associated SNP resides within overlapping TF binding sites for TFs with sex specific expression profiles. For example, consider a case in which TF A is expressed only in males and binds preferentially to the A allele at an eQTL SNP, whereas TF B is expressed only in females and binds preferentially to the G allele at the same SNP. If both TFs are activators of expression, such an occurrence could explain the sex-specificity for the directionality of the eQTL in this example.

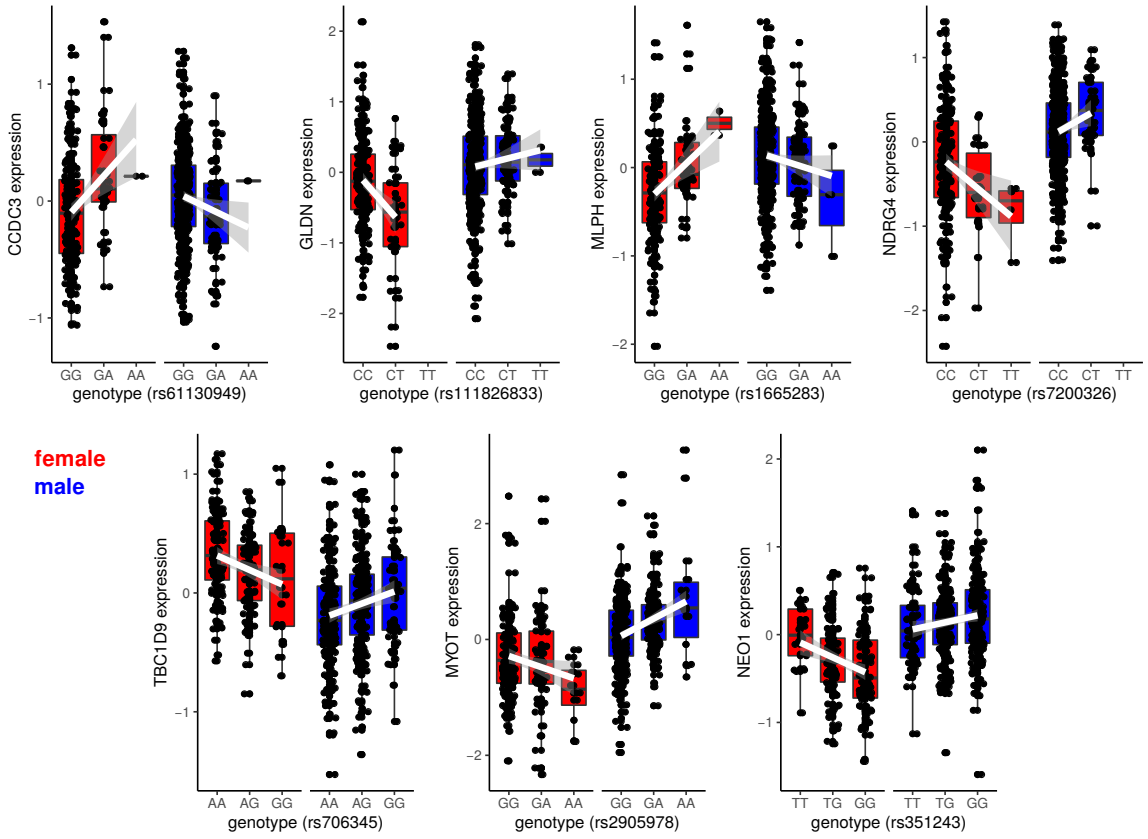

Figure S9: Sex-specific eQTL associations for sex-biased genes. Here we show the sex-specific eQTL profiles for 7/13 genes with both association loci and differential expression (related to main text Fig 6).

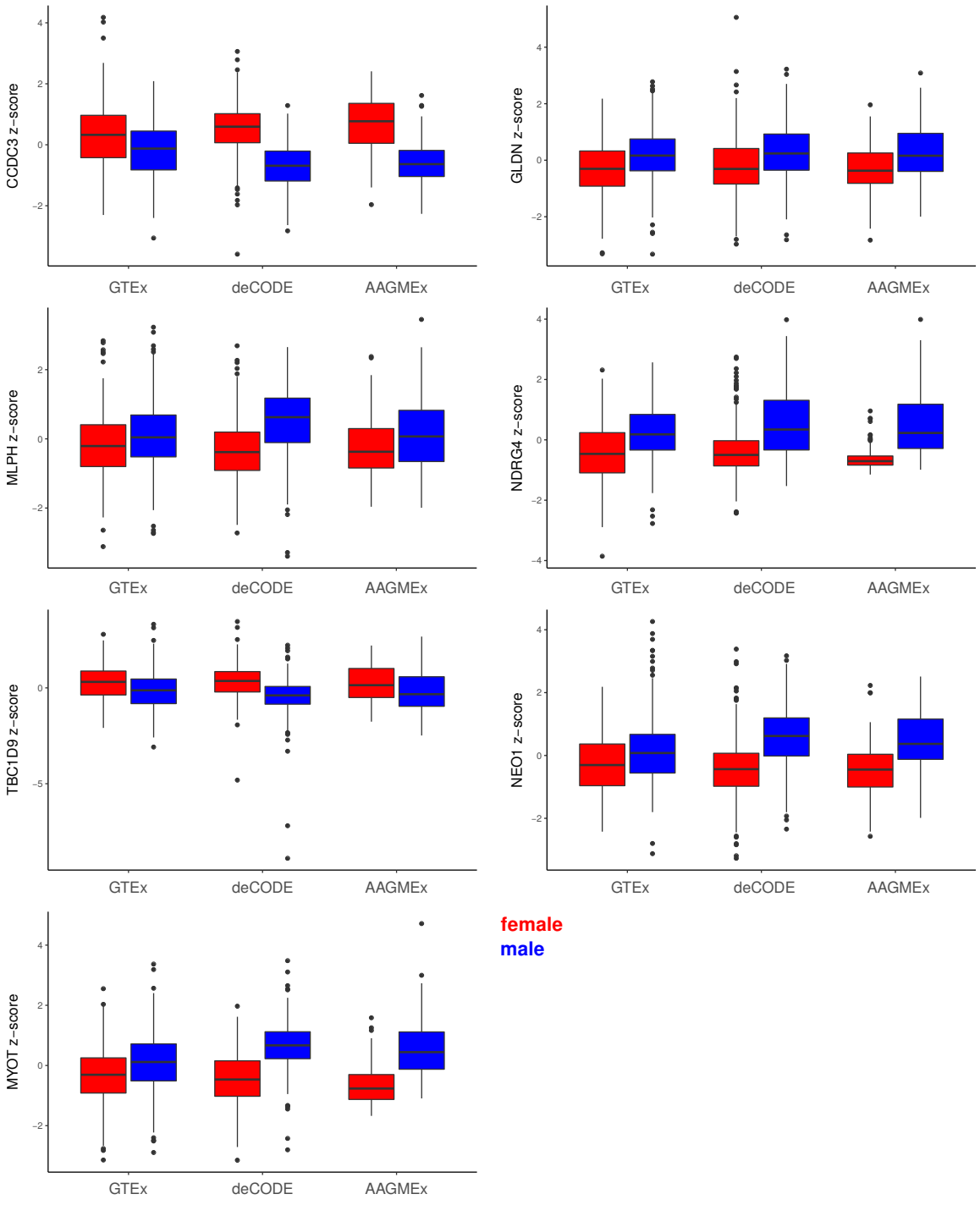

Figure S10: Differential expression profiles for genes with sex-specific eQTLs. Here we show the sex-biased expression profiles for 7/13 genes with both association loci and differential expression (related to main text Fig 6). The three data groupings correspond to the multi-ethnic (GTEx), Icelandic (deCODE), and African American (AAGMEx) cohorts, from left the right, respectively.

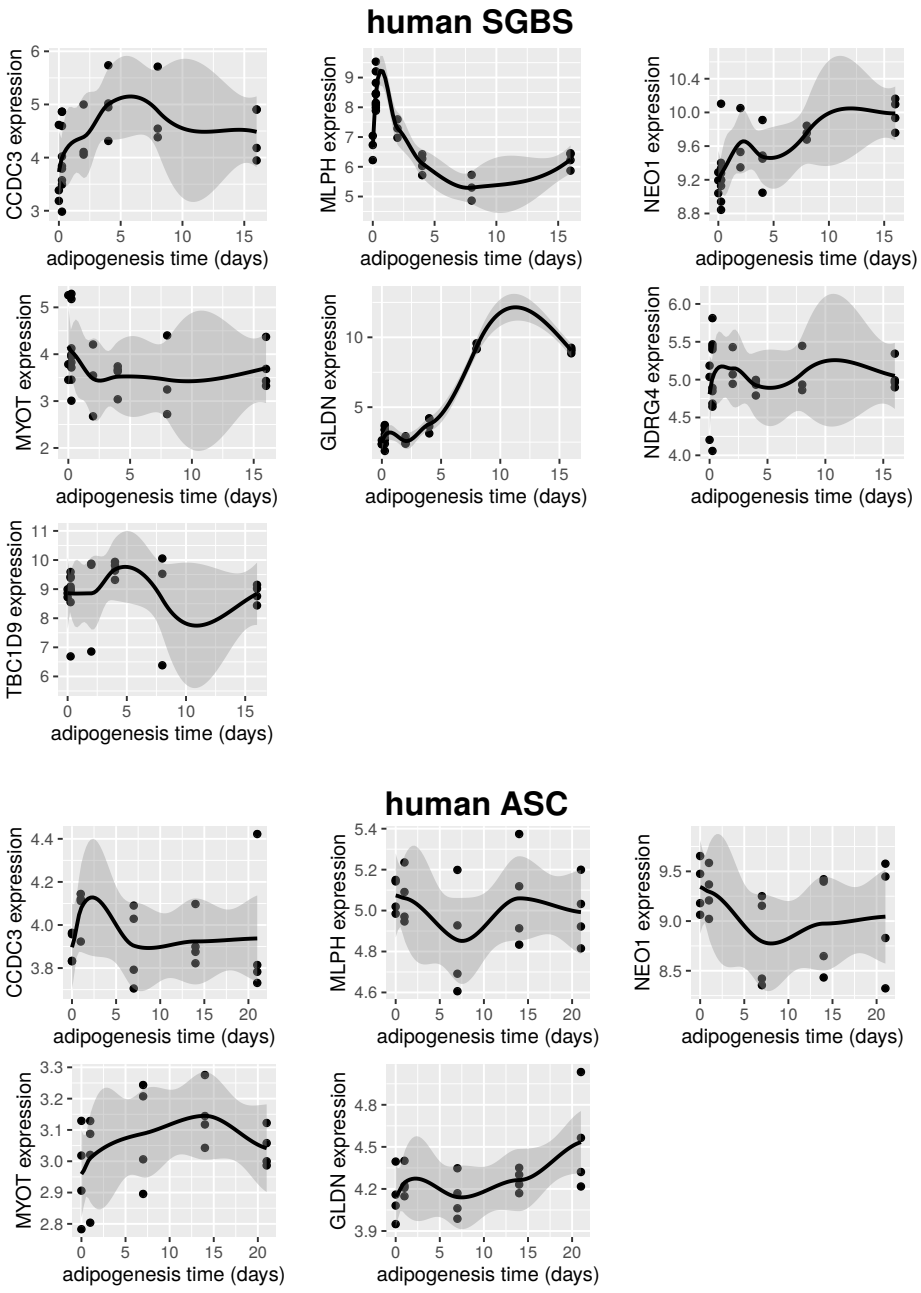

Figure S11: Human adipogenesis of genes with sex-biased expression and sex-specific eQTLs. Here we show the temporal dynamics of gene expression, throughout adipogenesis, for 7/13 genes with both association loci and differential expression (related to main text Fig 7). Data are shown for the SGBS cell line and adipose stromal cell-derived pre-adipocytes (ASC).

References

Ambele MA, Dessels C, Durandt C, and Pepper MS. 2016. Genome-wide analysis of gene expression during adipogenesis in human adipose-derived stromal cells reveals novel patterns of gene expression during adipocyte differentiation. *Stem Cell Research* **16**: 725–734.

Anderson LA, McTernan PG, Barnett AH, and Kumar S. 2001. The effects of androgens and estrogens on preadipocyte proliferation in human adipose tissue: influence of gender and site. *The Journal of Clinical Endocrinology and Metabolism* **86**: 5045–5051.

Arner P and Spalding KL. 2010. Fat cell turnover in humans. *Biochemical and Biophysical Research Communications* **396**: 101–104.

Arroyo JD, Jourdain AA, Calvo SE, Ballarano CA, Doench JG, Root DE, and Mootha VK. 2016. A Genome-wide CRISPR Death Screen Identifies Genes Essential for Oxidative Phosphorylation. *Cell Metabolism* **24**: 875–885.

Bayindir-Buchhalter I, Wolff G, Lerch S, Sijmonsma T, Schuster M, Gronych J, Billeter AT, Babaei R, Krunic D, Ketscher L, et al.. 2018. Cited4 is a sex-biased mediator of the antidiabetic glitazone response in adipocyte progenitors. *EMBO molecular medicine* **10**.

Benjamini Y and Hochberg Y. 1995. Controlling the False Discovery Rate: A Practical and Powerful Approach to Multiple Testing. *Journal of the Royal Statistical Society. Series B (Methodological)* **57**: 289–300.

Bernard S, Frisén J, and Spalding KL. 2010. A mathematical model for the interpretation of nuclear bomb test derived 14C incorporation in biological systems. *Nuclear Instruments and Methods in Physics Research Section B: Beam Interactions with Materials and Atoms* **268**: 1295–1298.

Blouin K, Nadeau M, Perreault M, Veilleux A, Drolet R, Marceau P, Mailloux J, Luu-The V, and Tchernof A. 2010. Effects of androgens on adipocyte differentiation and adipose tissue explant metabolism in men and women. *Clinical Endocrinology* **72**: 176–188.

Broman KW, Keller MP, Broman AT, Kendziorski C, Yandell BS, Sen and Attie AD. 2015. Identification and Correction of Sample Mix-Ups in Expression Genetic Data: A Case Study. *G3 (Bethesda, Md.)* **5**: 2177–2186.

Brookes ST, Whitely E, Egger M, Smith GD, Mulheran PA, and Peters TJ. 2004. Subgroup analyses in randomized trials: risks of subgroup-specific analyses; power and sample size for the interaction test. *Journal of Clinical Epidemiology* **57**: 229–236.

Buniello A, MacArthur JAL, Cerezo M, Harris LW, Hayhurst J, Malangone C, McMahon A, Morales J, Mountjoy E, Sollis E, et al.. 2019. The NHGRI-EBI GWAS Catalog of published genome-wide association studies, targeted arrays and summary statistics 2019. *Nucleic Acids Research* **47**: D1005–D1012.

Chen EY, Tan CM, Kou Y, Duan Q, Wang Z, Meirelles GV, Clark NR, and Ma'ayan A. 2013. Enrichr: interactive and collaborative HTML5 gene list enrichment analysis tool. *BMC bioinformatics* **14**: 128.

Chen X, Ayala I, Shannon C, Fourcaudot M, Acharya NK, Jenkinson CP, Heikkinen S, and Norton L. 2018. The Diabetes Gene and Wnt Pathway Effector TCF7L2 Regulates Adipocyte Development and Function. *Diabetes* **67**: 554–568.

Cheng H, Qi T, Zhang X, Kong Q, Min X, Mao Q, Cao X, Liu L, and Ding Z. 2019. Deficiency of heat shock protein A12A promotes browning of white adipose tissues in mice. *Biochimica Et Biophysica Acta. Molecular Basis of Disease* **1865**: 1451–1459.

Civelek M, Wu Y, Pan C, Raulerson CK, Ko A, He A, Tilford C, Saleem NK, Stančáková A, Scott LJ, et al.. 2017. Genetic Regulation of Adipose Gene Expression and Cardio-Metabolic Traits. *American Journal of Human Genetics* **100**: 428–443.

Contreras GA, Thelen K, Ayala-Lopez N, and Watts SW. 2016. The distribution and adipogenic potential of perivascular adipose tissue adipocyte progenitors is dependent on sexual dimorphism and vessel location. *Physiological Reports* **4**.

Dahlman I, Linder K, Arvidsson Nordström E, Andersson I, Lidén J, Verdich C, Sørensen TIA, and Arner P. 2005. Changes in adipose tissue gene expression with energy-restricted diets in obese women. *The American Journal of Clinical Nutrition* **81**: 1275–1285.

Dahlman I, Mejhert N, Linder K, Agustsson T, Mutch DM, Kulyte A, Isaksson B, Permert J, Petrovic N, Nedergaard J, et al.. 2010. Adipose tissue pathways involved in weight loss of cancer cachexia. *British Journal of Cancer* **102**: 1541–1548.

Danecek P, Auton A, Abecasis G, Albers CA, Banks E, DePristo MA, Handsaker RE, Lunter G, Marth GT, Sherry ST, et al.. 2011. The variant call format and VCFtools. *Bioinformatics (Oxford, England)* **27**: 2156–2158.

Deplancke B, Alpern D, and Gardeux V. 2016. The Genetics of Transcription Factor DNA Binding Variation. *Cell* **166**: 538–554.

Dieudonne MN, Pecquery R, Leneveu MC, and Giudicelli Y. 2000. Opposite effects of androgens and estrogens on adipogenesis in rat preadipocytes: evidence for sex and site-related specificities and possible involvement of insulin-like growth factor 1 receptor and peroxisome proliferator-activated receptor gamma2. *Endocrinology* **141**: 649–656.

Elbein SC, Kern PA, Rasouli N, Yao-Borengasser A, Sharma NK, and Das SK. 2011. Global Gene Expression Profiles of Subcutaneous Adipose and Muscle From Glucose-Tolerant, Insulin-Sensitive, and Insulin-Resistant Individuals Matched for BMI. *Diabetes* **60**: 1019–1029.

ENCODE Project Consortium. 2012. An integrated encyclopedia of DNA elements in the human genome. *Nature* **489**: 57–74.

Ernst J and Kellis M. 2012. ChromHMM: automating chromatin-state discovery and characterization. *Nature Methods* **9**: 215–216.

Fisher RA. 1922. On the Interpretation of 2 from Contingency Tables, and the Calculation of P. *Journal of the Royal Statistical Society* **85**: 87–94.

Foulley JL. 2000. A completion simulator for the two-sided truncated normal distribution. *Genetics, Selection, Evolution : GSE* **32**: 631–635.

Frankish A, Diekhans M, Ferreira AM, Johnson R, Jungreis I, Loveland J, Mudge JM, Sisu C, Wright J, Armstrong J, et al.. 2019. GENCODE reference annotation for the human and mouse genomes. *Nucleic Acids Research* **47**: D766–D773.

Franzén O, Ermel R, Cohain A, Akers NK, Di Narzo A, Talukdar HA, Foroughi-Asl H, Giambartolomei C, Fullard JF, Sukhavasi K, et al.. 2016. Cardiometabolic Risk Loci Share Downstream Cis- and Trans-Gene Regulation Across Tissues and Diseases. *Science (New York, N.Y.)* **353**: 827–830.

Gaignard P, Fréchou M, Liere P, Thérond P, Schumacher M, Slama A, and Guennoun R. 2018. Sex differences in brain mitochondrial metabolism: influence of endogenous steroids and stroke. *Journal of Neuroendocrinology* **30**.

Ghaben AL and Scherer PE. 2019. Adipogenesis and metabolic health. *Nature Reviews. Molecular Cell Biology* **20**: 242–258.

Gilks WP, Abbott JK, and Morrow EH. 2014. Sex differences in disease genetics: evidence, evolution, and detection. *Trends in Genetics* **30**: 453–463.

Greenawalt DM, Dobrin R, Chudin E, Hatoum IJ, Suver C, Beaulaurier J, Zhang B, Castro V, Zhu J, Sieberts SK, et al.. 2011. A survey of the genetics of stomach, liver, and adipose gene expression from a morbidly obese cohort. *Genome Research* **21**: 1008–1016.

Gromovsky AD, Schugar RC, Brown AL, Helsley RN, Burrows AC, Ferguson D, Zhang R, Sansbury BE, Lee RG, Morton RE, et al.. 2018. -5 Fatty Acid Desaturase FADS1 Impacts Metabolic Disease by Balancing Proinflammatory and Proresolving Lipid Mediators. *Arteriosclerosis, Thrombosis, and Vascular Biology* **38**: 218–231.

GTEx Consortium, Laboratory, Data Analysis &Coordinating Center (LDACC)—Analysis Working Group, Statistical Methods groups—Analysis Working Group, Enhancing GTEx (eGTEx) groups, NIH Common Fund, NIH/NCI, NIH/NHGRI, NIH/NIMH, NIH/NIDA, Biospecimen Collection Source Site—NDRI, et al.. 2017. Genetic effects on gene expression across human tissues. *Nature* **550**: 204–213.

Guo H, Zhang L, Zhu C, Yang F, Wang S, Zhu S, and Ma X. 2017. A Single Nucleotide Polymorphism in the FADS1 Gene is Associated with Plasma Fatty Acid and Lipid Profiles and Might Explain Gender Difference in Body Fat Distribution. *Lipids in Health and Disease* **16**.

Gupta V, Bhasin S, Guo W, Singh R, Miki R, Chauhan P, Choong K, Tchkonia T, Lebrasseur NK, Flanagan JN, et al.. 2008. Effects of dihydrotestosterone on differentiation and proliferation of human mesenchymal stem cells and preadipocytes. *Molecular and Cellular Endocrinology* **296**: 32–40.

Gérard D, Schmidt F, Ginolhac A, Schmitz M, Halder R, Ebert P, Schulz MH, Sauter T, and Sinkkonen L. 2019. Temporal enhancer profiling of parallel lineages identifies AHR and GLIS1 as regulators of mesenchymal multipotency. *Nucleic Acids Research* **47**: 1141–1163.

Ho DSW, Schierding W, Wake M, Saffery R, and O'Sullivan J. 2019. Machine Learning SNP Based Prediction for Precision Medicine. *Frontiers in Genetics* **10**.

't Hoen PAC, Friedländer MR, Almlöf J, Sammeth M, Pulyakhina I, Anvar SY, Laros JFJ, Buermans HPJ, Karlberg O, Brännvall M, et al.. 2013. Reproducibility of high-throughput mRNA and small RNA sequencing across laboratories. *Nature Biotechnology* **31**: 1015–1022.

Howie B, Marchini J, and Stephens M. 2011. Genotype imputation with thousands of genomes. *G3 (Bethesda, Md.)* **1**: 457–470.

Hu W, Jiang C, Guan D, Dierickx P, Zhang R, Moscati A, Nadkarni GN, Steger DJ, Loos RJF, Hu C, et al.. 2019. Patient Adipose Stem Cell-Derived Adipocytes Reveal Genetic Variation that Predicts Antidiabetic Drug Response. *Cell Stem Cell* **24**: 299–308.e6.

Jiménez-Mateos EM, González-Billault C, Dawson HN, Vitek MP, and Avila J. 2006. Role of MAP1B in axonal retrograde transport of mitochondria. *The Biochemical Journal* **397**: 53–59.

Kadoki M, Patil A, Thaiss CC, Brooks DJ, Pandey S, Deep D, Alvarez D, von Andrian UH, Wagers AJ, Nakai K, et al.. 2017. Organism-Level Analysis of Vaccination Reveals Networks of Protection across Tissues. *Cell* **171**: 398–413.e21.

Keuper M, Berti L, Raedle B, Sachs S, Böhm A, Fritsche L, Fritsche A, Häring HU, Hrabě de Angelis M, Jastroch M, et al.. 2019. Preadipocytes of obese humans display gender-specific bioenergetic responses to glucose and insulin. *Molecular Metabolism* **20**: 28–37.

Khramtsova EA, Davis LK, and Stranger BE. 2019. The role of sex in the genomics of human complex traits. *Nature Reviews. Genetics* **20**: 173–190.

Kudryavtseva E, Forde TS, Pucker AD, and Adarichev VA. 2012. Wnt signaling genes of murine chromosome 15 are involved in sex-affected pathways of inflammatory arthritis. *Arthritis and Rheumatism* **64**: 1057–1068.

Kuleshov MV, Jones MR, Rouillard AD, Fernandez NF, Duan Q, Wang Z, Koplev S, Jenkins SL, Jagodnik KM, Lachmann A, et al.. 2016. Enrichr: a comprehensive gene set enrichment analysis web server 2016 update. *Nucleic Acids Research* **44**: W90–97.

Lachmann A, Xu H, Krishnan J, Berger SI, Mazloom AR, and Ma'ayan A. 2010. ChEA: transcription factor regulation inferred from integrating genome-wide ChIP-X experiments. *Bioinformatics (Oxford, England)* **26**: 2438–2444.

Leek JT and Storey JD. 2007. Capturing heterogeneity in gene expression studies by surrogate variable analysis. *PLoS genetics* **3**: 1724–1735.

Liberzon A, Birger C, Thorvaldsdóttir H, Ghandi M, Mesirov JP, and Tamayo P. 2015. The Molecular Signatures Database (MSigDB) hallmark gene set collection. *Cell Systems* **1**: 417–425.

Lippert C, Listgarten J, Liu Y, Kadie CM, Davidson RI, and Heckerman D. 2011. FaST linear mixed models for genome-wide association studies. *Nature Methods* **8**: 833–835.

Listgarten J, Kadie C, Schadt EE, and Heckerman D. 2010. Correction for hidden confounders in the genetic analysis of gene expression. *Proceedings of the National Academy of Sciences of the United States of America* **107**: 16465–16470.

Lo KA, Labadorf A, Kennedy NJ, Han MS, Yap YS, Matthews B, Xin X, Sun L, Davis RJ, Lodish HF, et al.. 2013. Analysis of in vitro insulin-resistance models and their physiological relevance to in vivo diet-induced adipose insulin resistance. *Cell Reports* **5**: 259–270.

Love MI, Huber W, and Anders S. 2014. Moderated estimation of fold change and dispersion for RNA-seq data with DESeq2. *Genome Biology* **15**: 550.

Lusis AJ, Seldin MM, Allayee H, Bennett BJ, Civelek M, Davis RC, Eskin E, Farber CR, Hui S, Mehrabian M, et al.. 2016. The Hybrid Mouse Diversity Panel: a resource for systems genetics analyses of metabolic and cardiovascular traits. *Journal of Lipid Research* **57**: 925–942.

Lê KA, Mahurkar S, Alderete TL, Hasson RE, Adam TC, Kim JS, Beale E, Xie C, Greenberg AS, Allayee H, et al.. 2011. Subcutaneous adipose tissue macrophage infiltration is associated with hepatic and visceral fat deposition, hyperinsulinemia, and stimulation of NF-B stress pathway. *Diabetes* **60**: 2802–2809.

Maher AC, Fu MH, Isfort RJ, Varbanov AR, Qu XA, and Tarnopolsky MA. 2009. Sex Differences in Global mRNA Content of Human Skeletal Muscle. *PLoS ONE* **4**.

Min SY, Desai A, Yang Z, Sharma A, Genga RMJ, Kucukural A, Lifshitz L, Maehr R, Garber M, and Corvera S. 2019. "Multiple human adipocyte subtypes and mechanisms of their development". *bioRxiv* p. 537464.

Mootha VK, Lindgren CM, Eriksson KF, Subramanian A, Sihag S, Lehar J, Puigserver P, Carlsson E, Ridderstråle M, Laurila E, et al.. 2003. PGC-1alpha-responsive genes involved in oxidative phosphorylation are coordinately downregulated in human diabetes. *Nature Genetics* **34**: 267–273.

Nassiri I, Lombardo R, Lauria M, Morine MJ, Moyseos P, Varma V, Nolen GT, Knox B, Sloper D, Kaput J, et al.. 2016. Systems view of adipogenesis via novel omics-driven and tissue-specific activity scoring of network functional modules. *Scientific Reports* **6**: 28851.

Norheim F, Hasin-Brumshtein Y, Vergnes L, Chella Krishnan K, Pan C, Seldin MM, Hui ST, Mehrabian M, Zhou Z, Gupta S, et al.. 2019. Gene-by-Sex Interactions in Mitochondrial Functions and Cardio-Metabolic Traits. *Cell Metabolism* **29**: 932–949.e4.

Pan DZ, Garske KM, Alvarez M, Bhagat YV, Boocock J, Nikkola E, Miao Z, Raulerson CK, Cantor RM, Civelek M, et al.. 2018. Integration of human adipocyte chromosomal interactions with adipose gene expression prioritizes obesity-related genes from GWAS. *Nature Communications* **9**: 1512.

Patterson N, Price AL, and Reich D. 2006. Population structure and eigenanalysis. *PLoS genetics* **2**: e190.

Perfilyev A, Dahlman I, Gillberg L, Rosqvist F, Iggman D, Volkov P, Nilsson E, Risérus U, and Ling C. 2017. Impact of polyunsaturated and saturated fat overfeeding on the DNA-methylation pattern in human adipose tissue: a randomized controlled trial. *The American Journal of Clinical Nutrition* **105**: 991–1000.

Price AL, Patterson NJ, Plenge RM, Weinblatt ME, Shadick NA, and Reich D. 2006. Principal components analysis corrects for stratification in genome-wide association studies. *Nature Genetics* **38**: 904–909.

Pulit SL, Stoneman C, Morris AP, Wood AR, Glastonbury CA, Tyrrell J, Yengo L, Ferreira T, Marouli E, Ji Y, et al.. 2019. Meta-analysis of genome-wide association studies for body fat distribution in 694 649 individuals of European ancestry. *Human Molecular Genetics* **28**: 166–174.

Purcell S, Neale B, Todd-Brown K, Thomas L, Ferreira MAR, Bender D, Maller J, Sklar P, de Bakker PIW, Daly MJ, et al.. 2007. PLINK: a tool set for whole-genome association and population-based linkage analyses. *American Journal of Human Genetics* **81**: 559–575.

R Core Team. 2018. *R: A Language and Environment for Statistical Computing*. R Foundation for Statistical Computing, Vienna, Austria.

Ralston JC, Matravadia S, Gaudio N, Holloway GP, and Mutch DM. 2015. Polyunsaturated fatty acid regulation of adipocyte FADS1 and FADS2 expression and function. *Obesity (Silver Spring, Md.)* **23**: 725–728.

Rask-Andersen M, Karlsson T, Ek WE, and Johansson 2019. Genome-wide association study of body fat distribution identifies adiposity loci and sex-specific genetic effects. *Nature Communications* **10**: 339.

Reich DE, Cargill M, Bolk S, Ireland J, Sabeti PC, Richter DJ, Lavery T, Kouyoumjian R, Farhadian SF, Ward R, et al.. 2001. Linkage disequilibrium in the human genome. *Nature* **411**: 199–204.

Ritchie ME, Phipson B, Wu D, Hu Y, Law CW, Shi W, and Smyth GK. 2015. limma powers differential expression analyses for RNA-sequencing and microarray studies. *Nucleic Acids Research* **43**: e47.

Roadmap Epigenomics Consortium, Kundaje A, Meuleman W, Ernst J, Bilenky M, Yen A, Heravi-Moussavi A, Kheradpour P, Zhang Z, Wang J, et al.. 2015. Integrative analysis of 111 reference human epigenomes. *Nature* **518**: 317–330.

Rodriguez-Cuenca S, Pujol E, Justo R, Frontera M, Oliver J, Gianotti M, and Roca P. 2002. Sex-dependent thermogenesis, differences in mitochondrial morphology and function, and adrenergic response in brown adipose tissue. *The Journal of Biological Chemistry* **277**: 42958–42963.

Rosen ED and Spiegelman BM. 2014. What we talk about when we talk about fat. *Cell* **156**: 20–44.

Shabalin AA. 2012. Matrix eQTL: ultra fast eQTL analysis via large matrix operations. *Bioinformatics (Oxford, England)* **28**: 1353–1358.

Siersbæk R, Madsen JGS, Javierre BM, Nielsen R, Bagge EK, Cairns J, Wingett SW, Traynor S, Spivakov M, Fraser P, et al.. 2017. Dynamic Rewiring of Promoter-Anchored Chromatin Loops during Adipocyte Differentiation. *Molecular Cell* **66**: 420–435.e5.

Silaidos C, Pilatus U, Grewal R, Matura S, Lienerth B, Pantel J, and Eckert GP. 2018. Sex-associated differences in mitochondrial function in human peripheral blood mononuclear cells (PBMCs) and brain. *Biology of Sex Differences* **9**: 34.

Singh R, Artaza JN, Taylor WE, Braga M, Yuan X, Gonzalez-Cadavid NF, and Bhasin S. ???? Testosterone inhibits adipogenic differentiation in 3T3-L1 cells: nuclear translocation of androgen receptor complex with beta-catenin and T-cell factor 4 may bypass canonical Wnt signaling to down-regulate adipogenic transcription factors. *Endocrinology* **147**.

Small KS, Todorčević M, Civelek M, El-Sayed Moustafa JS, Wang X, Simon MM, Fernandez-Tajes J, Mahajan A, Horikoshi M, Hugill A, et al.. 2018. Regulatory variants at KLF14 influence type 2 diabetes risk via a female-specific effect on adipocyte size and body composition. *Nature Genetics* **50**: 572–580.

Spalding KL, Arner E, Westermark PO, Bernard S, Buchholz BA, Bergmann O, Blomqvist L, Hoffstedt J, Näslund E, Britton T, et al.. 2008. Dynamics of fat cell turnover in humans. *Nature* **453**: 783–787.

Stegle O, Parts L, Piipari M, Winn J, and Durbin R. 2012. Using probabilistic estimation of expression residuals (PEER) to obtain increased power and interpretability of gene expression analyses. *Nature Protocols* **7**: 500–507.

Subramanian A, Tamayo P, Mootha VK, Mukherjee S, Ebert BL, Gillette MA, Paulovich A, Pomeroy SL, Golub TR, Lander ES, et al.. 2005. Gene set enrichment analysis: a knowledge-based approach for interpreting genome-wide expression profiles. *Proceedings of the National Academy of Sciences of the United States of America* **102**: 15545–15550.

Tareen SHK, Adriaens ME, Arts ICW, de Kok TM, Vink RG, Roumans NJT, van Baak MA, Mariman ECM, Evelo CT, and Kutmon M. 2018. Profiling Cellular Processes in Adipose Tissue during Weight Loss Using Time Series Gene Expression. *Genes* **9**.

Tchoukalova YD, Koutsari C, Votruba SB, Tchkonia T, Giorgadze N, Thomou T, Kirkland JL, and Jensen MD. 2010. Sex- and depot-dependent differences in adipogenesis in normal-weight humans. *Obesity (Silver Spring, Md.)* **18**: 1875–1880.

Tewhey R, Kotliar D, Park DS, Liu B, Winnicki S, Reilly SK, Andersen KG, Mikkelsen TS, Lander ES, Schaffner SF, et al.. 2016. Direct Identification of Hundreds of Expression-Modulating Variants using a Multiplexed Reporter Assay. *Cell* **165**: 1519–1529.

Toker L, Feng M, and Pavlidis P. 2016. Whose sample is it anyway? Widespread misannotation of samples in transcriptomics studies. *F1000Research* **5**.

Vadigepalli R, Chakravarthula P, Zak DE, Schwaber JS, and Gonye GE. 2003. PAINT: a promoter analysis and interaction network generation tool for gene regulatory network identification. *Omics: A Journal of Integrative Biology* **7**: 235–252.

Viguerie N, Montastier E, Maoret JJ, Roussel B, Combes M, Valle C, Villa-Vialaneix N, Iacovoni JS, Martinez JA, Holst C, et al.. 2012. Determinants of human adipose tissue gene expression: impact of diet, sex, metabolic status, and cis genetic regulation. *PLoS genetics* **8**: e1002959.

Vijay V, Han T, Moland CL, Kwekel JC, Fuscoe JC, and Desai VG. 2015. Sexual dimorphism in the expression of mitochondria-related genes in rat heart at different ages. *PloS One* **10**: e0117047.

Vishvanath L and Gupta RK. 2019. Contribution of adipogenesis to healthy adipose tissue expansion in obesity. *The Journal of Clinical Investigation* **129**: 4022–4031.

Wang S, Zang C, Xiao T, Fan J, Mei S, Qin Q, Wu Q, Li X, Xu K, He HH, et al.. 2016. Modeling cis-regulation with a compendium of genome-wide histone H3K27ac profiles. *Genome Research* **26**: 1417–1429.

Wang Z, Civelek M, Miller CL, Sheffield NC, Guertin MJ, and Zang C. 2018. BART: a transcription factor prediction tool with query gene sets or epigenomic profiles. *Bioinformatics (Oxford, England)* **34**: 2867–2869.

Yao C, Joehanes R, Johnson AD, Huan T, Esko T, Ying S, Freedman JE, Murabito J, Lunetta KL, Metspalu A, et al.. 2014. Sex- and age-interacting eQTLs in human complex diseases. *Human Molecular Genetics* **23**: 1947–1956.

Yin X, Lanza IR, Swain JM, Sarr MG, Nair KS, and Jensen MD. 2014. Adipocyte mitochondrial function is reduced in human obesity independent of fat cell size. *The Journal of Clinical Endocrinology and Metabolism* **99**: E209–216.

Zhang X, Chen X, Qi T, Kong Q, Cheng H, Cao X, Li Y, Li C, Liu L, and Ding Z. 2019. HSPA12A is required for adipocyte differentiation and diet-induced obesity through a positive feedback regulation with PPAR. *Cell Death and Differentiation* **26**: 2253–2267.

Zhang Y, Yu H, Gao P, Chen J, Yu C, Zong C, Lu S, Li X, Ma X, Liu Y, et al.. 2016. The Effect of Growth Hormone on Lipid Accumulation or Maturation in Adipocytes. *Cellular Physiology and Biochemistry: International Journal of Experimental Cellular Physiology, Biochemistry, and Pharmacology* **39**: 2135–2148.